Chapter 5
Interaction of Surface Plasmon Polaritons with Nanomaterials

Gagan Kumar and Prashant K. Sarswat

Abstract Surface plasmon polaritons are the surface electromagnetic excitations that exist at the metal-air or metal-dielectric interface. Because of their enhanced field and strong confinement near the metal surface, they offer variety of applications ranging from high sensitivity sensors to miniaturized photonic components. In this chapter, we present analytical formalisms of several optical phenomenon that occur in their interaction with nanomaterials and analyze their significance in absorption, enhanced Raman scattering, electron acceleration, optical fiber sensors etc. First, we discuss dispersion properties of surface plasmon polaritons in single and double metal film configurations. The analysis is extended to the examination of dispersion properties of multilayer thin film configurations. We also present dispersion properties of surface plasmon polaritons in thin film metal coated optical fibers and develop an analytical formalism for the calculation of amplitude of the laser mode converted surface plasmon wave. The chapter also presents a theoretical model for surface plasmon polariton assisted electron acceleration in thin film metal configuration. Furthermore, surface plasmon polariton interactions with metallic nanoparticles are examined and analytical formalism of their anomalous absorption by nanoparticles is presented. In this context, we present surface plasmon assisted surface enhanced Raman scattering by the molecules when they are adsorbed on nanoparticles.

Keywords Surface plasmons • Nanomaterials • Electron acceleration • Optical fibers • Surface enhanced Raman scattering • Anomalous absorption

G. Kumar (✉)
Department of Physics, Indian Institute of Technology Guwahati, Guwahati 781039, Assam, India
e-mail: gk@iitg.ernet.in

P.K. Sarswat
Department of Metallurgical Engineering, University of Utah, Salt Lake City, UT 84112, USA
e-mail: prashant.sarswat@utah.edu

C.D. Geddes (ed.), *Reviews in Plasmonics 2015*,
DOI 10.1007/978-3-319-24606-2_5

5.1 Introduction

Surface plasmon polaritons (SPPs) are the guided electromagnetic waves that propagates along the interface between a metal and a dielectric, often a vacuum [1]. The amplitude of the SPPs decays exponentially away from the interface in both the media. The magnetic field of the SPPs is parallel to the surface and perpendicular to its direction of propagation while electric field has components parallel to the direction of propagation and perpendicular to the surface. Surface waves were first observed by Wood in 1902 [2]. He noted anomalous behavior in the diffraction intensities for small angular and spectral variations from the grating of large and rapid changes. In 1907, Rayleigh gave the first theoretical explanation of these anomalies suggesting that such behavior was due to the cutoff or the appearance of a new spectral order [3]. However, more precisely Fano in 1941, theoretically suggested the excitation of surface plasmon polaritons over the grating surface [4]. He pointed out that such wave can be excited only by transverse magnetic (TM) incident wave and exists only at the interface of a dielectric and a medium with negative real part of effective relative permittivity viz. plasma and conductor. Major developments in the excitation of surface plasmon waves over solid state plasmas took place in 1968 when Otto proposed the SPPs excitation in attenuated total reflection (ATR) configuration [5]. Kretschmann and Raether [6] later proposed an alternative configuration of Otto's method.

The SPPs offers a variety of applications, ranging from high sensitivity sensors to supplementary heating in a fusion reactor, coherent radiation generation, enhanced material ablation, electron emission, and plasma diagnostics. Surface plasmons are confined near the metal surface and its amplitude at the surface is significantly larger than that of the laser. The enhanced field of the SPPs could increase the emission rate of luminescent dyes placed near the metal surface. This enhancement can increase the efficiency and the brightness of solid-state LEDs [7]. In last two decades, surface plasmon based sensors have emerged as a powerful tool for characterizing and quantifying bimolecular interactions. Surface plasmon polaritons are being explored for their potential in sub-wavelength optics, magneto-optic data storage, and microscopy [8]. The properties of surface plasmon polaritons can lead to miniaturized photonic circuits by creatively designing the structure of metal's surface. In this chapter, we will discuss the dispersion properties of the surface plasmon polaritons over the metal-air and metal-dielectric interfaces, and analyze their significance in absorption, electron acceleration, optical fiber sensors, and surface enhanced Raman scattering.

5.2 Dispersion Properties of Surface Plasmon Polaritons

5.2.1 Dispersion Relation Over a Single Metal Surface

The fields of the SPPs at metal-dielectric interface are governed by Maxwell's equations in each medium and the associated boundary conditions. Boundary conditions involve the continuity of the tangential component of the electric field

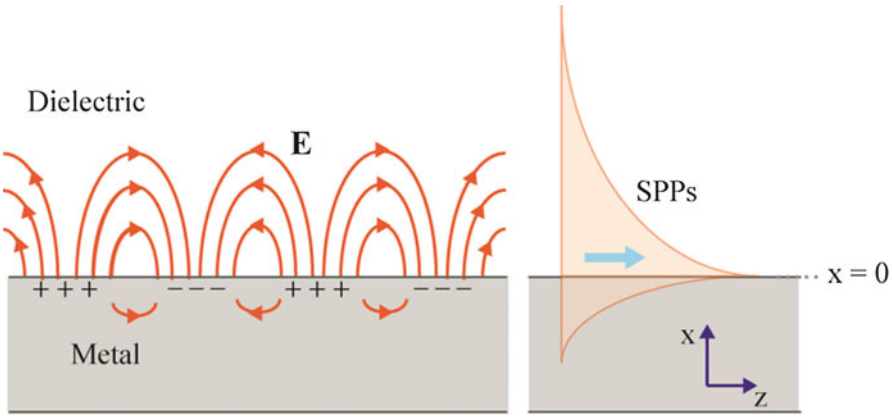

Fig. 5.1 Geometry of surface plasmon polaritons propagation at metal-air interface

and magnetic fields across the interface and vanishing of these fields away from the interface.

Consider a dielectric of relative permittivity ε_1 for $x > 0$ and a metal with effective relative permittivity $\varepsilon(\omega)$ in the half space $x < 0$ (Fig. 5.1). When a SPP propagates at the dielectric-metal interface with (t, z) variation as $e^{-i(\omega t - k_z z)}$, its behavior is governed by Maxwell's equations.

$$\nabla \times \vec{\boldsymbol{E}} = -\frac{1}{c}\frac{\partial \vec{\boldsymbol{H}}}{\partial t}, \tag{5.1}$$

$$\nabla \times \vec{\mathbf{H}} = \frac{\varepsilon'}{c}\frac{\partial \vec{\mathbf{E}}}{\partial t}, \tag{5.2}$$

which on taking curl of Eq. (5.1) and using Eq. (5.2) give

$$\nabla^2 \vec{\boldsymbol{E}} - \frac{\varepsilon'}{c^2}\frac{\partial^2 \vec{\boldsymbol{E}}}{\partial t^2} = 0, \tag{5.3}$$

where $\varepsilon' = \varepsilon(\omega) = \varepsilon_L - \omega_P^2/\omega^2$ for $x < 0$ and $\varepsilon' = \varepsilon_1$ for $x > 0$. ε_L is the lattice permittivity, ω_P is the plasma frequency. The continuity conditions on electromagnetic fields at the interface demand that the t and z variation of fields be the same in both media. Thus replacing $\partial/\partial z$ and $\partial/\partial t$ in Eq. (5.3) by ik_z and $-i\omega$ respectively, we get

$$\frac{\partial^2 \vec{E}}{\partial x^2} - \left(k_z^2 - \frac{\omega^2}{c^2}\varepsilon'\right)\vec{E} = 0. \tag{5.4}$$

The well behaved solutions of Eq. (5.4) are

$$\begin{aligned} \vec{E} &= \left(\hat{z} + \hat{x}\frac{ik_z}{\alpha_1}\right) Ae^{-\alpha_1 x} e^{-i(\omega t - k_z z)}, \quad \text{for} \quad x > 0, \\ \vec{E} &= \left(\hat{z} - \hat{x}\frac{ik_z}{\alpha_2}\right) Ae^{\alpha_2 x} e^{-i(\omega t - k_z z)}, \quad \text{for} \quad x < 0. \end{aligned} \tag{5.5}$$

where $\alpha_1^2 = k_z^2 - \varepsilon_1\omega^2/c^2$, $\alpha_2^2 = k_z^2 - \omega^2\varepsilon(\omega)/c^2$. The real part of α_1, α_2 must be positive for an electromagnetic wave localized to the dielectric-metal interface at x = 0. The continuity of E_z and $\varepsilon' E_x$ at the interface yields $A = B$,

$$\frac{\alpha_2}{\alpha_1} = -\frac{\varepsilon(\omega)}{\varepsilon_1}. \tag{5.6}$$

Squaring both sides and rearranging the terms, one obtains the explicit dispersion relation for surface plasma polaritons

$$k_{SPP} = \frac{\omega}{c}\left(\frac{\varepsilon_1\varepsilon(\omega)}{\varepsilon_1 + \varepsilon(\omega)}\right)^{1/2}. \tag{5.7}$$

Further, $\alpha_1^2 = -\frac{\omega^2}{c^2}\frac{\varepsilon_1^2}{\varepsilon_1+\varepsilon}$, $\alpha_2^2 = -\frac{\omega^2}{c^2}\frac{\varepsilon^2}{\varepsilon_1+\varepsilon}$. For α_1 and α_2 to be positive one needs $\varepsilon_1 + \varepsilon < 0$ or $\omega < \frac{\omega_P}{\sqrt{\varepsilon_L+\varepsilon_1}}$. In case of metal-free space interface, the surface plasmons dispersion relation reduces to $k_z = \frac{\omega}{c}\left(\frac{\varepsilon}{1+\varepsilon}\right)^{1/2}$. We have plotted the dispersion relation at dielectric-metal and air-metal interfaces in Fig. 5.2 for the parameters: $\varepsilon_1 = 2.25, \varepsilon_L = 4$. One may note that as the wavenumber increases, dispersion curve shifted away from the light line and finally saturates at high wavenumber value. It may be noted that the surface plasmon polaritons wavenumber increases with ε_1.

5.2.2 *Dispersion Relation of SPPs in Double Metal Surface Configuration*

The excitation of symmetric surface plasmon polartons in a double metal surface configuration is important in a variety of applications such as biochemical sensing, line narrowing of spectral features, and electron acceleration etc. Therefore it is

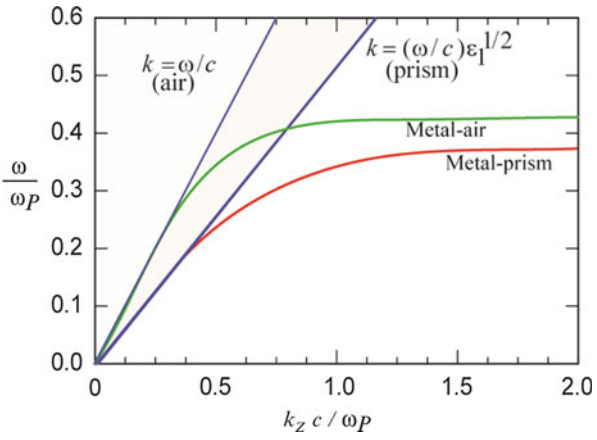

Fig. 5.2 Dispersion relations for surface plasmon polaritons at metal-air and metal prism interfaces

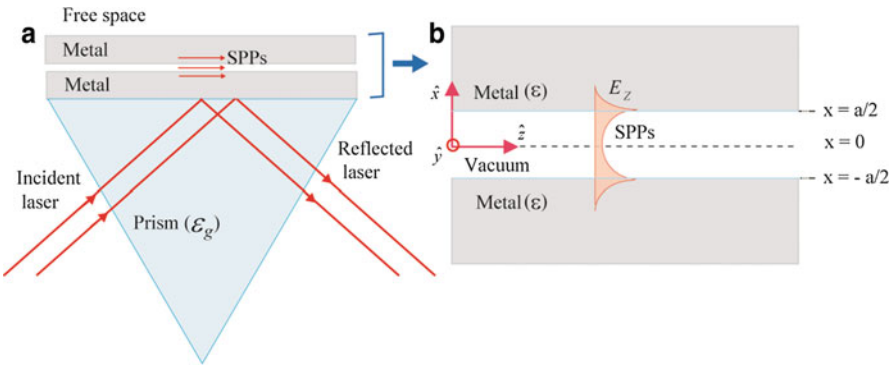

Fig. 5.3 Schematic of two metal surface plasmon structure. The metal surfaces at x = −a/2 and x = a/2 are separated by free space. The surface plasmon polaritons are excited via attenuated total reflection (*ATR*) configuration

crucial to understand the propagation properties of the surface plasmon polariton excitations in this configuration. Consider two parallel metal half spaces $x < -a/2$ and $x > a/2$, separated by a thin vacuum region $-a/2 < x < a/2$ as shown in Fig. 5.3. The effective permittivity of metal at frequency ω is $\varepsilon = \varepsilon_L - \omega_P^2/\omega^2$, where ε_L is the lattice permittivity and ω_P is the plasma frequency.

Surface plasmons propagate through two metal configuration with t, z variation as $\exp[-i(\omega t - k_z z)]$. The field variations are governed by Maxwell's third and fourth equations given by Eqs. (5.1) and (5.2) with

$$\begin{aligned} \varepsilon' &= 1 \quad \text{for} \quad -a/2 < x < a/2 \\ &= \varepsilon \quad \text{for} \quad x < -a/2 \quad \text{and} \quad x > a/2 \end{aligned}$$

As discussed earlier, taking curl of Maxwell's third equation and using fourth, we obtain wave equation. The wave equation governing E_z in three media is given by Eq. (5.4). The well behaved solution of Eq. (5.4), satisfying $\nabla . \vec{E} = 0$ in each region is

$$\begin{aligned} \vec{E} &= A\left(\hat{z} + \hat{x}\frac{ik_z}{\alpha_1}\right) e^{-\alpha_1 x}, && x > a/2, \\ &= \left[A_1\left(\hat{z} - \hat{x}\frac{ik_z}{\alpha_2}\right) e^{\alpha_2 x} + A_2\left(\hat{z} + \hat{x}\frac{ik_z}{\alpha_2}\right) e^{-\alpha_2 x}\right], && -a/2 < x < a/2, \\ &= A_3\left(\hat{z} - \hat{x}\frac{ik_z}{\alpha_1}\right) e^{\alpha_1 x}, && x < -a/2, \end{aligned} \tag{5.8}$$

Where $\alpha_1 = \left(k_z^2 - \omega^2\varepsilon/c^2\right)^{1/2}$, $\alpha_2 = \left(k_z^2 - \omega^2/c^2\right)^{1/2}$. Applying conditions of continuity of E_z and $\varepsilon' E_x$ at $x = a/2$ and $-a/2$, we get

$$
\begin{aligned}
A_1\, e^{\alpha_2 a/2} + A_2\, e^{-\alpha_2 a/2} &= A\, e^{-\alpha_1 a/2},\\
A_1\, e^{\alpha_2 a/2} - A_2\, e^{-\alpha_2 a/2} &= -A\left(\frac{\varepsilon\alpha_2}{\alpha_1}\right) e^{-\alpha_1 a/2},\\
A_1\, e^{-\alpha_2 a/2} + A_2\, e^{\alpha_2 a/2} &= A_3\, e^{-\alpha_1 a/2},\\
A_1\, e^{-\alpha_2 a/2} - A_2\, e^{\alpha_2 a/2} &= A_3\left(\frac{\varepsilon\alpha_2}{\alpha_1}\right) e^{-\alpha_1 a/2}.
\end{aligned}
\tag{5.9}
$$

Solving these equations, we obtain the dispersion relation

$$
\frac{\alpha_2^2}{\alpha_1^2} = \left|\frac{1 - e^{\alpha_2 a}}{1 + e^{\alpha_2 a}}\right|^2 \frac{1}{|\varepsilon|^2}. \tag{5.10}
$$

Using dimensionless quantities: $q = k_z c\ /\omega_P, \Omega = \omega/\omega_P, a^{'} = a\omega_P/c$, Eq. (5.10) is normalized and plotted normalized frequency Ω versus normalized wavenumber q in Fig. 5.4 for the mode that has E_x symmetric about the $x = 0$ $(A_1 = -A_2)$. The parameters are: $\varepsilon_L = 1$, $a\omega_P/c = 100$. From the figure, one may note that as the wave number increases, frequency increases and then saturates at higher wave numbers. For higher value of wave number q, the behavior of the curve is same as that of single metal surface structure. However in double metal surface, at lower value of wave number phase velocity is smaller. The phenomenon of reducing phase velocity can be useful in achieving wave electron synchronization at lower electron energies and hence accelerating electrons.

5.2.3 *Surface Plasmons in Multilayer Thin Films Configuration*

In case of metal-insulator-metal (MIM) configuration, surface plasmons are correlated with natural electromagnetic mode of the structures that can be obtained from Maxwell's equation solution using proper boundary conditions. The modes propagation behavior relies on permittivity of each layer. In case of multilayer structures, various analytical models and numerical methods have been utilized for the analysis of the splitting modes [9]. Other methods such as Eigen function [10] treatment and semi-analytical mode matching technique were also utilized for the analysis of the one dimensional photonic crystals and scattering of surface plasmons at abrupt surface (metal-dielectric interface), respectively [11]. Such analysis becomes more and more difficult when number of layers is increased. In order to find dispersion relation for these intricate problems, matrix method have been used, where one diagonal term is set as zero [12].

In case of multilayered structures, dielectric layers are aligned in XY plane. As each layer has a constant electric permittivity, it will result in a piecewise continuous solution. Knowing the fact that surface plasmons are excited due to presence

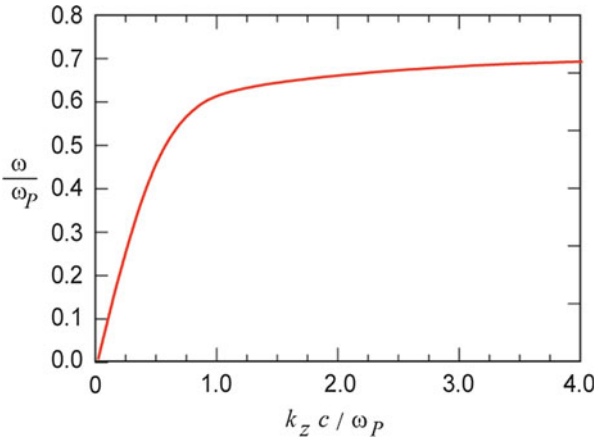

Fig. 5.4 Variation of normalized frequency $\Omega = \omega/\omega_P$ versus normalized wave number $q = k_z c/\omega_P$ of the surface plasmon polaritons in double metal surface configuration. The parameters are: $\varepsilon_L = 1$, $a\omega_P/c = 100$.

of perpendicular electric field or its component with respect to surface, electric field components are considered in X-Z plane and magnetic field is considered in Y direction. Let us consider Eqs. (5.1) and (5.2) again, if their 'x' dependence is considered as $\exp(i\alpha_n x)$ for the representation of a wave, traveling in positive 'x' direction, its magnetic field variation along z direction can be represented as [12]

$$\alpha_n^2 u_n(z) = \varepsilon(z)k^2 u_n(z) + \varepsilon(z)\left[\frac{1}{\varepsilon(z)}\frac{d^2u_n(z)}{dz^2} + \frac{du_n(z)}{dz}\frac{d}{dz}\left(\frac{1}{\varepsilon(z)}\right)\right], \tag{5.11}$$

where, $u_n(z)$ is the nth eigenfunction and α_n [2] is corresponding n^{th} eigenvalue. As mentioned earlier that it is a piecewise continuous, the solution of Eq. (5.11) can be written as

$$u_n(z) = \sum \left(H_{n,l}^{+} e^{\left(i\gamma_{n,l}\left(z-z_l^0\right)\right)} + H_{n,l}^{-} e^{-\left(i\gamma_{n,l}\left(z-z_l^0\right)\right)}\right) \quad \text{(Summed over } l\text{)}\,, \tag{5.12}$$

where, z_l^0 is the location of the lower boundary for layer 'l'. $H_{n,l}^{+}$ and $H_{n,l}^{-}$ are the amplitudes of upward and downward propagating waves, respectively. The corresponding wavenumber for each layer, $\gamma_{n,l}$ can be evaluated as:

$$\gamma_{n,l} = \pm\sqrt{\varepsilon_l k^2 - \alpha_n^2}. \tag{5.13}$$

One should be careful while choosing the sign of $\gamma_{n,l}$. This sign should be chosen such that the imaginary part will always be positive, in order to ensure that there will be a decay in wave amplitude when it propagate. It is important to note that coefficients have different value for different layer but for a particular layer these coefficients will be constant. The magnetic field can be written as [12]

$$H(r,\omega) = \vec{Y}\sum \left(H_{n,l}^{+} e^{\left(i\gamma_{n,l}\left(z-z_l^0\right)\right)} + H_{n,l}^{-} e^{-\left(i\gamma_{n,l}\left(z-z_l^0\right)\right)}\right) e^{i\alpha_n x} \quad \text{(Summed over } l\text{)}, \tag{5.14}$$

Similarly, for electric field:

$$E(r,\omega) = e^{i\alpha_n x}\sum \left(\frac{1}{k\varepsilon_l}{}^{l} H_{n,l}^{+}\left(\gamma_{n,l}\hat{x} - \alpha_n \hat{z}\right) e^{\left(i\gamma_{n,l}\left(z-z_l^0\right)\right)} - \frac{1}{k\varepsilon_l} H_{n,l}^{-}\left(\gamma_{n,l}\hat{x} + \alpha_n \hat{z}\right) e^{-\left(i\gamma_{n,l}\left(z-z_l^0\right)\right)}\right), \tag{5.15}$$

Across the layer, tangential components of field are continuous, α_n will be treated as a constant for entire structure. Also, $H_{n,l}^{+}$ and $H_{n,l}^{-}$ in particular layer 'l' are linked to other coefficients in adjacent layers. Considering the boundary condition, x-component of electric field and magnetic field between two adjacent layers (l and $l+1$) can be matched using following matrix equation [12]

$$\begin{bmatrix} H_{n,l+1}^{+} \\ H_{n,l+1}^{-} \end{bmatrix} = \frac{1}{2}\begin{bmatrix} 1 & \dfrac{\varepsilon_{l+1}}{\gamma_{n,l+1}} \\ 1 & -\dfrac{\varepsilon_{l+1}}{\gamma_{n,l+1}} \end{bmatrix}\begin{bmatrix} 1 & 1 \\ \dfrac{\gamma_{n,l}}{\varepsilon_l} & -\dfrac{\gamma_{n,l}}{\varepsilon_l} \end{bmatrix} \times \begin{bmatrix} e^{i\gamma_{n,l}t_l} & 0 \\ 0 & e^{-i\gamma_{n,l}t_l} \end{bmatrix}\begin{bmatrix} H_{n,l}^{+} \\ H_{n,l}^{-} \end{bmatrix}, \tag{5.16}$$

where, the thickness of layer 'l' is t_l . Using Eq. (5.16), correlation between adjacent layers can be established and magnetic field can be obtained in entire structure by multiplying matrix for individual layer. Hence, magnetic field at lowest layer ($l=0$) can be linked with magnetic field at a generalized ($l=L$) layer

$$\begin{bmatrix} H_{n,L}^{+} \\ H_{n,L}^{-} \end{bmatrix} = \begin{bmatrix} A_{11} & A_{12} \\ A_{21} & A_{22} \end{bmatrix}\begin{bmatrix} H_{n,0}^{+} \\ H_{n,0}^{-} \end{bmatrix}, \tag{5.17}$$

where, A_{xx} ($x=1$ or 2) are matrix elements. Now, for the top most layer and in absence of incident field: $H_{n,0}^{+} = H_{n,L}^{-} = 0$. For outward directed field: $H_{n,L}^{+} = A_{12}\, H_{n,0}^{-}$; $0 = A_{22}\ H_{n,0}^{-}$, that gives $A_{22} = 0$; This is a constrain that is responsible for discrete set of surface plasmon modes in the structure. It is important to note that solution of these equations can be found using numerical methods. However, dispersion relation for single metal surface and thin film can be verified as follows

For a single metal dielectric combination, $L=1$, it can be written [12]

$$\begin{bmatrix} H_{n,1}^{+} \\ H_{n,1}^{-} \end{bmatrix} = \frac{1}{2}\begin{bmatrix} 1 & \dfrac{\varepsilon_1}{\gamma_{n,1}} \\ 1 & -\dfrac{\varepsilon_1}{\gamma_{n,1}} \end{bmatrix}\begin{bmatrix} 1 & 1 \\ \dfrac{\gamma_{n,0}}{\varepsilon_l} & -\dfrac{\gamma_{n,0}}{\varepsilon_l} \end{bmatrix} \times \begin{bmatrix} 1 & 0 \\ 0 & 1 \end{bmatrix}\begin{bmatrix} H_{n,0}^{+} \\ H_{n,0}^{-} \end{bmatrix}. \tag{5.18}$$

Further simplification gives

$$\begin{bmatrix} H_{n,1}^{+} \\ H_{n,1}^{-} \end{bmatrix} = \frac{1}{2} \begin{bmatrix} 1 + \dfrac{\varepsilon_1 \gamma_{n,0}}{\gamma_{n,1} \varepsilon_0} & 1 - \dfrac{\varepsilon_1 \gamma_{n,0}}{\gamma_{n,1} \varepsilon_0} \\ 1 - \dfrac{\varepsilon_1 \gamma_{n,0}}{\gamma_{n,1} \varepsilon_0} & 1 + \dfrac{\varepsilon_1 \gamma_{n,0}}{\gamma_{n,1} \varepsilon_0} \end{bmatrix} \times \begin{bmatrix} 1 & 0 \\ 0 & 1 \end{bmatrix} \begin{bmatrix} H_{n,0}^{+} \\ H_{n,0}^{-} \end{bmatrix}. \tag{5.19}$$

$$\text{It indicates } \mathrm{A}_{22} = \frac{1}{2} \left[1 + \frac{\varepsilon_1 \gamma_{n,0}}{\gamma_{n,1} \varepsilon_0} \right]. \tag{5.20}$$

Using relation $\mathrm{A}_{22} = 0$, Eq. (5.20) can be written as

$$\left[1 + \frac{\varepsilon_1}{\sqrt{\varepsilon_1 k^2 - \alpha_n^2}} \frac{\sqrt{\varepsilon_0 k^2 - \alpha_n^2}}{\varepsilon_0} \right] = 0. \tag{5.21}$$

Solving for α_n, we obtain

$$\alpha = \pm k \left[\frac{\varepsilon_1 \varepsilon_0}{\varepsilon_1 + \varepsilon_0} \right]^{\frac{1}{2}}. \tag{5.22}$$

This is an established dispersion relation already discussed in Sect. 5.1 through Eq. (5.7).

5.3 Absorption of Surface Plasmons Polaritons by Metallic Nanoparticles

The absorption of laser radiation at material surfaces is significant to material ablation [13] and other applications. The optical absorption is very poor for smooth metal surfaces because the high free electron density of metals renders effective plasma permittivity to be negative and surface re-radiates light energy in the surrounding medium. However, for the metallic particles, absorption of the electromagnetic waves could be significantly high when the wave frequency is close to the natural frequency of oscillations of the electron cloud. The total absorption of electromagnetic wave can be achieved through the excitation of surface plasmon polaritons [1, 14]. Experiments have revealed total absorption of femtosecond laser due to surface modifications via the generation of surface electromagnetic waves [15]. In this section, we will understand the mechanism by which the total absorption of the surface electromagnetic waves can be achieved through the excitation of surface plasmon polaritons.

Consider a metal free-space interface ($x = 0$) with metal occupying half space ($x < 0$) and free space is $x > 0$ (cf. Fig. 5.5). The metal is having spherical particles

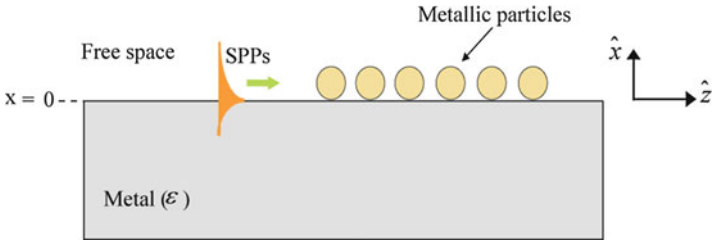

Fig. 5.5 Schematic for the absorption of surface plasmon polaritons by metallic particles adsorbed on metal surface

of size r_c and aerial density N per unit surface area, are placed over it. The effective relative permittivity ε of the metal is given as

$$\varepsilon = \left(\varepsilon_L - \frac{\omega_P^2}{\omega^2}\right) + i\,\frac{\gamma}{\omega}\,\frac{\omega_P^2}{\omega^2}, \tag{5.23}$$

where ω is the incident laser frequency. ε_L is the lattice permittivity, ω_P is the plasma frequency and γ is the electron phonon collision frequency in the metal film. Suppose a surface plasmon propagates through the configuration with field variation given by $\boldsymbol{E}_S = \boldsymbol{A}_S\, exp[-i(\omega t - k_z z)]$. The amplitude $\boldsymbol{A}_S$ in metal and free space regions are given by Eq. (5.5). The dispersion relation of surface plasmon polaritons as discussed in the earlier section is given by

$$k_{sp} = \frac{\omega}{c}\left(\frac{\varepsilon(\omega)}{1+\varepsilon(\omega)}\right)^{1/2}.$$

The surface plasmon polaritons decay with z over a propagation length (inverse of imaginary part of k_{sp})

$$L = {k_{si}}^{-1} = \frac{2\omega}{\gamma}\,\frac{\omega_P^2}{\omega^2}\left(\frac{\omega_P^2}{\omega^2} - \varepsilon_L - 1\right)^{1/2}\left(\frac{\omega_P^2}{\omega^2} - \varepsilon_L\right)^{1/2}. \tag{5.24}$$

When the surface plasmons field in the free space region interacts with the metal particle having internal electron density n_e, then the response of electrons of a particle is governed by equation of motion

$$m\frac{d^2\boldsymbol{s}}{dt^2} = -e\boldsymbol{E}_S - m\gamma\,\boldsymbol{v} - \frac{m\omega_{Pe}^2\,\boldsymbol{s}}{3}, \tag{5.25}$$

where '$\boldsymbol{s}$' is the displacement of electrons of the particle from equilibrium, $\boldsymbol{v} = d\boldsymbol{s}/dt$ is their velocity, m and $-e$ are the electronic mass and charge, ω_{Pe} is the plasma frequency of the metal particle which is same as ω_P when the metal particle and metal

film are of same material. Taking x-component of Eq. (5.25), the velocity of the electron in x-direction turns out to be

$$v_x = \frac{e\,A\,\omega\,(k/\alpha_1)e^{-i\omega t}}{m\left(\omega^2 - \omega_{Pe}^2/3 + i\gamma\omega\right)}. \tag{5.26}$$

Similarly taking z-component one obtains

$$v_z = \frac{-ie\,A\,\omega\,e^{-i\omega t}}{m\left(\omega^2 - \omega_{Pe}^2/3 + i\gamma\omega\right)}\,. \tag{5.27}$$

Under the influence of the SPPs field, the energy absorbed by an electron per second is

$$\Gamma_{abs} = \frac{1}{2}\,Re\left[-e\boldsymbol{E}_S^*.\,\boldsymbol{v}\right], \tag{5.28}$$

where $\boldsymbol{E}_S$ is the electric field and * denotes the complex conjugate. Using Eqs. (5.5), (5.26) and (5.27) in Eq. (5.28), along with boundary conditions yielding A = B, we obtain

$$\Gamma_{abs} = \frac{e^2\omega^2\,A^2\,\gamma\,\left(1 + k^2/\alpha_1^2\right)}{2m\left(\left(\omega^2 - \omega_{Pe}^2/3\right)^2 + \gamma^2\omega^2\right)}\,. \tag{5.29}$$

If n_0 is the electron density in the metal particle, then the power absorbed per second per particle is

$$\Gamma_{abs} = \frac{\omega_{Pe}^2\,A^2\,\omega^2\,\gamma\,\left(1 + k^2/\alpha_1^2\right)\,r_c^3}{6\left(\left(\omega^2 - \omega_{Pe}^2/3\right)^2 + \gamma^2\omega^2\right)}, \tag{5.30}$$

When N is the number of particles per unit area on the metal surface with inter particle separation $d = N^{-1/2} \geq r_c$, such that

$$N = \int n_P\,\delta(x - a)dx. \tag{5.31}$$

Then the energy absorbed in distance dz is

$$dP = -\Gamma_{abs}\,n_P\,dz, \tag{5.32}$$

$$= \frac{\omega_{Pe}^2\,A^2\,\omega^2\,\gamma\,\left(1 + k^2/\alpha_1^2\right)\,r_c}{6\left(\left(\omega^2 - \omega_{Pe}^2/3\right)^2 + \gamma^2\omega^2\right)}\left(\frac{r_c^2}{d^2}\right)dz. \tag{5.33}$$

Here P is the SPPs power flow per unit y width in the vacuum region

$$P = \frac{c}{4\pi}\int_0^{\infty} Re\left(\frac{\boldsymbol{E_S} \times \boldsymbol{H_S}}{2}\right)_z dx, \tag{5.34}$$

where $\boldsymbol{E_S}$, $\boldsymbol{H_S}$ are the electric and magnetic field intensity of the surface plasmon polaritons in the free space region. Using the third Maxwell's equation, we have $\boldsymbol{H_S} = (c/i\omega)(\nabla \times \boldsymbol{E_S})$. Submitting $\boldsymbol{E_S}$ and $\boldsymbol{H_S}$, we get

$$P = \frac{A^2\, c^2\, k\, \left(k^2/\alpha_1 - \alpha_1\right)}{16\, \pi\, \alpha_1^2\, \omega}\ , \tag{5.35}$$

From Eqs. (5.33) and (5.35), we obtain

$$\int_{P_0}^{P} \frac{dP}{P} = -\int_0^z k_{ip} dz + C, \tag{5.36}$$

giving $P = P_0\, e^{-k_{ip}\, z}$, where P_0 is the power at $z = 0$. The absorption constant k_{ip} is given as

$$k_{ip} = \frac{8\, \pi\, \omega_{Pe}^2\, \alpha_1^2\, \omega^3\, \gamma\, \left(1 + k^2/\alpha_1^2\right) r_c}{3\, k\, c^2 \left(\left(\omega^2 - \omega_{Pe}^2/3\right)^2 + \gamma^2\omega^2\right)\left(k^2/\alpha_1 - \alpha_1\right)} \frac{r_c^2}{d^2}\ , \tag{5.37}$$

One may note that the resonant enhancement in k_{ip} occurs at $\omega^2 = \omega_{Pe}^2/3$, corresponding to strong absorption of the wave. The resonant absorption depends upon the number density and the size of particles. In order to have numerical appreciation, normalized absorption constant k_{ip} versus $\delta/\omega_{Pe} = \left(\omega - \omega_{Pe}/\sqrt{3}\right)$ is plotted in Fig. 5.6 for two different particle sizes of $r_c = 6.5\ nm$ and $r_c = 8\ nm$ for the parameters: $\varepsilon = -5.5, \omega_{Pe} = 4.1 \times 10^{15}\ rad/sec\ , d = 112\ nm, \gamma = 7 \times 10^{12}\ sec^{-1}$.

5.4 Laser Mode Conversion into SPPs in a Metal Coated Optical Fiber

Fiber optic based sensors are important in a variety of applications including environmental monitoring, detection of bio-molecules and biochemical monitoring [16] etc. An optical fiber coated with silver or gold film instead of cladding have been employed for SPR (surface plasmon resonance) [17] and SERS (surface enhanced Raman scattering) sensor applications [18]. In this section, we examine how does the laser mode in a metal coated optical fiber converts to the surface plasmon polaritons. In our analytical formalism of mode conversion, we presume a

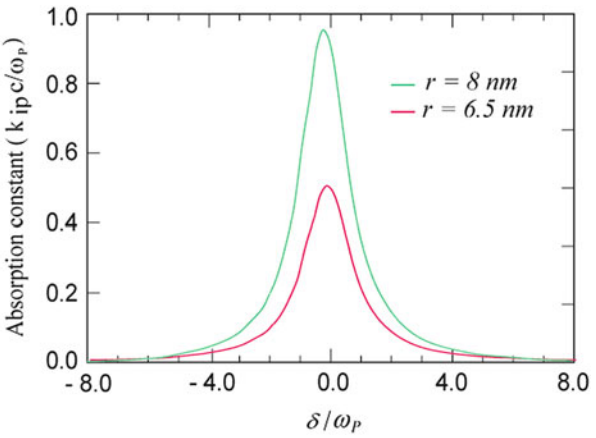

Fig. 5.6 Variation of normalized absorption constant, $k_{ip}c/\omega_{Pe}$ versus normalized frequency $\left(\omega - \omega_{Pe}/\sqrt{3}\right)/\omega_{Pe}$ for two particles of different size (i) $r_c = 6.5\ nm$ and (ii) $r_c = 8\ nm$ for the parameters: $\varepsilon = -5.5$, $\omega_{Pe} = 4.1 \times 10^{15}\ rad/sec$, $d = 112\ nm$, $\gamma = 7 \times 10^{12}\ sec^{-1}$.

ripple at the fiber metal interface to assist k-matching for the excitation of surface plasmon polaritons. When the body wave i.e. laser propagates through the fiber it induces oscillatory velocity to the electrons of the metal. The oscillatory velocity beats with the space modulated density to produce a current driving the surface plasmon polaritons on the metal free space interface. In our analysis we will first analyze the dispersion properties of surface plasmon polaritons and body waves followed by the mode conversion.

5.4.1 *Dispersion Relations of Body Waves and Surface Plasmon Polaritons*

Consider an optical fiber of radius 'a' and permittivity ε_g, coated with metal (a < r < b) of effective permittivity ε_m (cf. Fig. 5.7). The figure shows ripple at the glass-metal interface. Here we will confine our discussion to the dispersion relations of the body waves and surface plasmon waves. The role of ripple will be discussed in the next section of mode conversion.

A laser propagates through this structure in azimuthally symmetric TM mode with $t - z$ variation as $\exp[-i(\omega t - k_z z)]$. The propagation of field is governed by wave Eq. (5.3). The r-variation of fields in is given as

$$\frac{\partial^2 E_z}{\partial r^2} + \frac{1}{r}\frac{\partial E_z}{\partial r} + \left(\frac{\omega^2}{c^2}\varepsilon^{'} - {k_z}^2\right)E_z = 0, \tag{5.38}$$

where $\varepsilon' = \varepsilon_g$ for $r < a, \varepsilon^{'} = \varepsilon_m = \varepsilon_L - \omega_P^2/\omega(\omega + i\nu)$ for $a < r < b$, and $\varepsilon^{'} = 1$ for $r > b$. ε_L is the lattice permittivity. ω_P is the plasma frequency of free electrons inside the metal and γ is the electron collision frequency. The well behaved solutions of Eq. (5.38) in different regions are

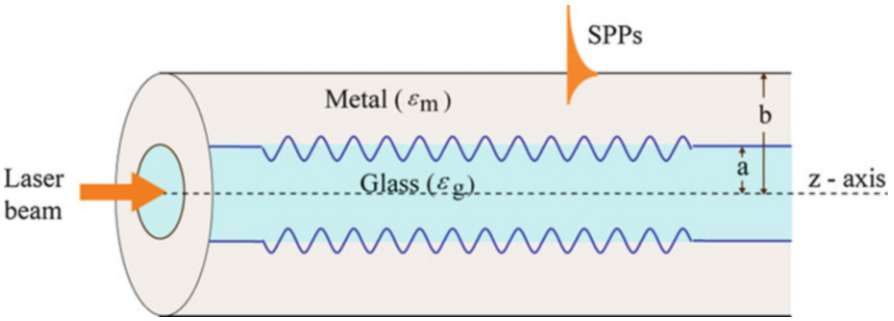

Fig. 5.7 Schematic of a metal coated optical fiber. The rippled interface between fiber and metal coating is used to assist k-matching for the conversion of a TM mode body wave to the surface plasmon polaritons

$$\begin{aligned}
\vec{E} &= A_1\left[J_0(k_\perp r)\hat{z} + \frac{ik_z}{k_\perp}J_0'(k_\perp r)\hat{r}\right]e^{-i(\omega t - k_z z)}, && 0 < r < a,\\
\vec{E} &= \left[(A_{21}I_0(\alpha_2 r) + A_{22}K_0(\alpha_2 r))\hat{z} - \left(\frac{ik_z}{\alpha_2}\right)\left(A_{21}I_0'(\alpha_2 r) + A_{22}K_0'(\alpha_2 r)\right)\hat{r}\right]e^{-i(\omega t - k_z z)}, && a < r < b,\\
\vec{E} &= A_3\left(K_0(\alpha_3 r)\hat{z} - \left(\frac{ik_z}{\alpha_3}\right)K_0'(\alpha_3 r)\hat{r}\right)e^{-i(\omega t - k_z z)}, && r > b,
\end{aligned} \tag{5.39}$$

where $k_\perp = \left(\frac{\omega^2\varepsilon_g}{c^2} - {k_z}^2\right)^{1/2}$, $\alpha_2 = \left({k_z}^2 - \frac{\omega^2\varepsilon_m}{c^2}\right)^{1/2}$, $\alpha_3 = \left({k_z}^2 - \frac{\omega^2}{c^2}\right)^{1/2}$ and the prime denotes differentiation w. r. t. argument. Continuity of E_z and $\varepsilon' E_r$ at $r = a, b$ demands

$$\begin{aligned}
A_{21}I_0(\alpha_2 a) + A_{22}K_0(\alpha_2 a) &= A_1 J_0(k_\perp a),\\
A_{21}I_0'(\alpha_2 a) + A_{22}K_0'(\alpha_2 a) &= -\left(\frac{\varepsilon_g\alpha_2}{\varepsilon_m k_\perp}\right)A_1 J_0'(k_\perp a),\\
A_{21}I_0(\alpha_2 b) + A_{22}K_0(\alpha_2 b) &= A_3 K_0(\alpha_3 b),\\
A_{21}I_0'(\alpha_2 b) + A_{22}K_0'(\alpha_2 b) &= \left(\frac{\alpha_2 A_3}{\varepsilon_m\alpha_3}\right)K_0'(\alpha_3 b).
\end{aligned} \tag{5.40}$$

leading to the dispersion relation

$$\left[J_0(k_\perp a) + \left(\frac{\alpha_2\varepsilon_g}{k_\perp\varepsilon_m}\right)\left(\frac{J_0'(k_\perp a)}{K_0'(\alpha_2 a)}\right)K_0(\alpha_2 a)\right]\left[I_0(\alpha_2 b) - \left(\frac{\alpha_3\varepsilon_m}{\alpha_2}\right)\left(\frac{I_0'(\alpha_2 b)}{K_0'(\alpha_3 b)}\right)K_0(\alpha_3 b)\right] = Q, \tag{5.41}$$

where,

$$Q = \frac{I_0'(\alpha_2 a)}{K_0'(\alpha_2 a)}\left[J_0(k_\perp a) + \frac{\alpha_2\varepsilon_g}{k_\perp\varepsilon_m}\frac{J_0'(k_\perp a)}{I_0'(\alpha_2 a)}I_0(\alpha_2 a)\right]\left[K_0(\alpha_2 b) - \frac{\alpha_3\varepsilon_m}{\alpha_2}\frac{K_0'(\alpha_2 b)}{K_0'(\alpha_3 b)}K_0(\alpha_3 b)\right]$$

In the limit $b \to \infty$ or $a \to 0$, $Q = 0$. In the former, the first factor in Eq. (5.41) equated to zero gives the body wave (TM mode)

$$J_0(k_\perp a) = -\frac{\alpha_2 \varepsilon_g}{k_\perp \varepsilon_m} \frac{J_0^{'}(k_\perp a)}{K_0^{'}(\alpha_2 a)} K_0(\alpha_2 a). \tag{5.42}$$

For $a \to 0$ the second factor in Eq. (5.41) equated to zero gives the surface plasmon polaritons propagation

$$I_0(\alpha_2 b) = \frac{\alpha_3 \varepsilon_m}{\alpha_2} \frac{I_0^{'}(\alpha_2 b)}{K_0^{'}(\alpha_3 b)} K_0(\alpha_3 b). \tag{5.43}$$

In the limit $b \to \infty$, Eq. (5.43) reduces to $\varepsilon_m = -\alpha_2/\alpha_3$, giving the usual dispersion relation for SPPs over a planar surface

$$k_z^2 = \frac{\omega^2}{c^2} \frac{\varepsilon_m}{\varepsilon_m + 1}. \tag{5.44}$$

In the general case when a and b are finite the modes are significantly modified by finite Q. In the case of much interest, $\alpha_2 b >> 1$, Q is small and the coupling between the two factors on the left of Eq. (5.41) is weak. Equation (5.41) admits another excitation of surface plasmon polaritons that propagates along glass-metal interface with dispersion relation

$$K_0(\alpha_2 a) = -\frac{\varepsilon_m}{\varepsilon_g} \frac{k_\perp}{\alpha_2} \frac{K_0^{'}(\alpha_2 a)}{J_0^{'}(k_\perp a)} J_0(k_\perp a), \tag{5.45}$$

In the limit $a \to \infty$, it takes the form $k_z^2 = (\omega^2/c^2)\left(\varepsilon_g \varepsilon_m/\left(\varepsilon_m + \varepsilon_g\right)\right)$. In Fig. 5.8, we have plotted normalized frequency $\Omega = \omega/\omega_P$ versus normalized wave number $q_z = k_z c/\omega_P$ for the Eqs. (5.42), (5.43) and (5.45) for the parameters: $\varepsilon_g = 2.13$, $\varepsilon_L = 10$, $b/a = 1.01$.

One may note that the frequency for TM mode begins with a cutoff and rises as q_z increases. The surface plasmon polartons have linear variation of Ω with q_z initially, however at large value of q_z, Ω tends to a saturation value. At a given Ω, the difference in q_z value for the TM mode and surface plasmon wave represents the wave number mismatch or the wave number required for resonant mode conversion. At $a\omega_P/c = 20$, one may calculate that a minimum of $q_z = 0.0184$ is required at $\Omega = 0.2453$ for the excitation of surface plasmon polaritons at the metal-free space interface. It is only in a narrow range of Ω, we can convert body wave into SPPs with a ripple of small q_z. Outside this range one would require a ripple of very high q_z, which is quite difficult to obtain.

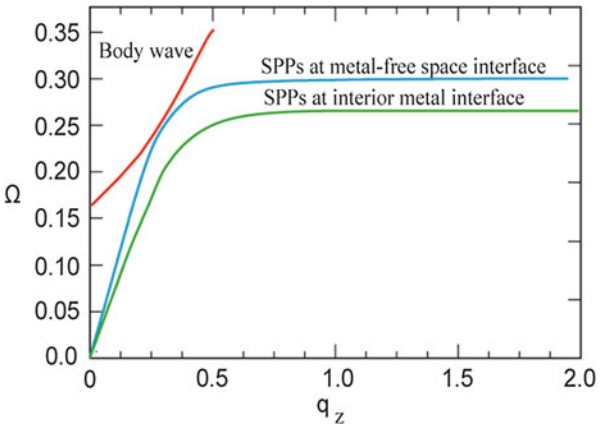

Fig. 5.8 Variation of normalized frequency, Ω with normalized wave number, q_z for TM mode body wave and SPPs. The parameters are: $\varepsilon_g = 2.13$, $\varepsilon_L = 10$, $a\omega_P/c = 20$, $b/a = 1.01$

5.4.2 Mode Conversion

Consider the fiber metal interface to be rippled (cf., Fig. 5.7), $r = a + h\cos(k_W z)$. On the outer side of the ripple, the electron density in the metal is n_0. In the ripple region $(a - h < r < a + h)$, it is periodic function of z, $n(z) = n(z + \lambda_W)$, where $\lambda_W = 2\pi/k_W$, h is the ripple wave amplitude and k_W is the ripple wave number.

Following Liu and Tripathi [19] we model the ripple by an electron density modulation,

$$n = \frac{n_0}{2}(1 + \sin(k_W z)), \quad \text{for} \quad a - h < r < a + h\,. \tag{5.46}$$

A laser of frequency ω_L and parallel wave number $k_z = k_L$ propagates through the fiber in TM mode. Its field in different regions is given by Eq. (5.39) with $A_S^{'}, k_\perp$, α_2, α_3 having a superfix L, designating laser. From Eq. (5.40), A_{21}^L, A_{22}^L, A_3^L are expressed in terms of A_1^L. Thus we may write the laser field as $\vec{E} = A_1^L\ \overrightarrow{\psi_L}(r)\exp(-i(\omega_L t - k_L z)$. This field imparts oscillatory velocity to electrons, $\vec{v} = e\vec{E}/mi\omega_L$, where $-e$ and m are the electronic charge and mass. Within the ripple region, $\vec{v}$ beats with n to produce a nonlinear current density at frequency ω_L and wave number $k_S = k_L + k_W$,

$$\vec{J}_S^{NL} = -\frac{n_0 e^2 A_1^L}{4mi\omega}\overrightarrow{\psi_L}\exp(-i(\omega_L t - k_S z)). \tag{5.47}$$

$\vec{J}_S^{NL}$ is localized in the ripple region and can be taken to be a delta function of r with $\overrightarrow{\psi_L}(r)$ replaced by $h\overrightarrow{\psi_L}(a)$. ω_L, k_S satisfy the dispersion relation for SPW, hence $\vec{J}_S^{NL}$ derive the surface plasmon polariton propagation. The relevant Maxwell's equations for the SPPs are

$$\begin{aligned}\nabla \times \vec{E}_S &= \left(\frac{i\omega_L}{c}\right)\vec{H}_S,\\ \nabla \times \vec{H}_S &= -\left(\frac{i\omega_L}{c}\right)\varepsilon'\vec{E}_S + \left(\frac{4\pi}{c}\right)\vec{J}_S^{NL}.\end{aligned} \tag{5.48}$$

Let the solution of these equations when $\vec{J}_S^{NL} = 0$ be $\vec{E}_{SO}$ and $\vec{H}_{SO}$, i. e.

$$\begin{aligned}\nabla \times \vec{E}_{SO} &= \left(\frac{i\omega_L}{c}\right)\vec{H}_{SO},\\ \nabla \times \vec{H}_{SO} &= -\left(\frac{i\omega_L}{c}\right)\varepsilon'\vec{E}_{SO}.\end{aligned} \tag{5.49}$$

$\vec{E}_{SO}$ is given by Eq. (5.39) with all $A's$, $\alpha_{2,}, \alpha_3$ having superscript s, denoting SPPs. Using Eq. (5.40), $A_{21}^s, A_{22}^s, A_3^s$ are expressible in terms of A_1^s. When $\vec{J}_S^{NL}$ is retained, let the fields, following Liu and Tripathi [19] be

$$\vec{E}_S = A(z)\,\vec{E}_{SO}(r,z,t), \quad \vec{H}_S = B(z)\,\vec{H}_{SO}(r,z,t). \tag{5.50}$$

Using these in Eq. (5.48) and employing Eq. (5.49), we obtain

$$\frac{\partial A}{\partial z}\hat{z} \times \vec{E}_{SO} = \frac{i\omega_L}{c}(B-A)\,\vec{H}_{SO}, \tag{5.51}$$

$$\frac{\partial B}{\partial z}\hat{z} \times \vec{H}_{SO} = \frac{i\omega_L}{c}\varepsilon'(B-A)\vec{E}_{SO} + \frac{4\pi}{c}\vec{J}_S^{NL}. \tag{5.52}$$

Multiplying Eq. (5.51) by $\vec{H}_{SO}{}^* rdr$, Eq. (5.52) by $\vec{E}_{SO}{}^* rdr$ and integrating over r from 0 to ∞, we get

$$\frac{\partial A}{\partial z} = +\frac{i\omega_L}{c}(B-A)\frac{P_2}{P_3{}^*}, \tag{5.53}$$

$$\frac{\partial B}{\partial z} = -\frac{i\omega_L}{c}(B-A)\frac{P_1}{P_3} + RA_1^L, \tag{5.54}$$

where $R = \dfrac{\pi n_0 e^2 h a}{c P_3 m i \omega_L}\,\vec{\psi}_L(a).\vec{\psi}_S{}^*(a)$, $\vec{E}_{so} = \vec{\psi}_s \exp[-i(\omega_L t - k_S z)]$,

$\vec{\psi}_L(a) = J_0(k_\perp a)\,\hat{z} + \frac{ik_z}{k_\perp}J_0'(k_\perp a)\,\hat{r}$, $\vec{\psi}_S(a) = I_0(\alpha_2 a)\,\hat{z} - \frac{ik_z}{\alpha_2}I_0'(\alpha_2 a)\,\hat{r}$,

$P_1 = \varepsilon'\int_0^\infty \vec{E}_{SO}.\vec{E}_{SO}{}^* rdr$, $P_2 = \int_0^\infty \vec{H}so.\vec{H}so^* rdr$, $P_3 = \int_0^\infty \left(\vec{E}_{SO}{}^* \times \vec{H}_{SO}\right)_z rdr$.

* denotes the complex conjugate. Equations (5.53) and (5.54), with initial conditions at $z = 0$, A = B = 0 give

$$\frac{A}{A_1^L} = \frac{R}{(1 + P_1P_3^*/P_2P_3)}\left(z + \left(e^{-i\gamma z} - 1\right)/i\gamma\right), \tag{5.55}$$

where $\gamma = (\omega_L/c)\,(P_1P_3^*/P_2P_3)$. This treatment is valid as long as $z < k_{si}^{-1}$, where k_{si}^{-1} is the absorption coefficient of the SPPs given by

$$k_{si} = \mathrm{Im}\left[\frac{\omega_L}{c}\left(\frac{\varepsilon_m}{1+\varepsilon_m}\right)^{1/2}\right]. \tag{5.56}$$

Putting $\varepsilon_m = \varepsilon_L - \omega_P^2/\omega_L\,(\omega_L + i\nu)$ in Eq. (5.56) we get

$$k_{si} = k_{SPW}\left(\frac{\omega_P^2\,\nu}{2\,{\omega_L}^3}\right)\frac{1}{\left[\omega_P^2/\omega_L^2 - (\varepsilon_L + 1)\right]\left[\omega_P^2/\omega_L^2 - \varepsilon_L\right]}, \tag{5.57}$$

where $k_{SPW} = (\omega_L/c)\left[\left(\omega_P^2/\omega_L^2 - \varepsilon_L\right)/\left(\omega_P^2/\omega_L^2 - (\varepsilon_L + 1)\right)\right]^{1/2}$, For $\gamma \approx 10^{12}\,s^{-1}$, $\varepsilon_L = 10$, $\omega_L/\omega_P = 0.2453$, then we obtain $z < 0.12\,cm$ for $\omega_L = 3.1970 \times 10^{15}\,rad/\sec$.

In order to have an appreciation of $|A|$ with z, we consider the case of frequency of the body wave, for a given $a\,\omega_P/c$, for which minimum ripple wave number is required. For $a\,\omega_P/c = 20$, this frequency is $\omega_L/\omega_P = \Omega = 0.2453$ with wave number $k_z\,c/\omega_P = q_z = 0.2727$ and corresponding ripple wave number $k_w\,c/\omega_P = q_w = 0.0184$. Also we use $\omega_L h/c \approx 0.2$. For these values, we get $P_1 = 3.5792\,cm^2$, $P_2 = 3.47176\,cm^2$, $P_3 = 2.34354\,cm^2$, $|R| = 47.214\,cm^{-1}$. This give $P_1P_3^*/P_2P_3 = 1.03 \cong 1$. Putting this value in Eq. (5.55) and taking modulus gives

$$\left|\frac{A}{A_L^1}\right| = \left[\left(\frac{|R|^2}{(\omega_L/c)^2}\right)\left(\frac{1}{4}\left(\frac{\omega_L z}{c} - \sin\left(\frac{\omega_L z}{c}\right)\right)^2 + \sin^4\left(\frac{\omega_L z}{2c}\right)\right)\right]^{1/2}. \tag{5.58}$$

Eq. (5.58) gives the ratio of amplitude of the surface plasma wave to the amplitude of the incident laser.

5.5 Electron Acceleration by Surface Plasmon Polaritons

The excitations of symmetric surface plasmon polaritons in double metal surface configuration as well as over a single metal surface have been discussed in the Sect. 5.1. In this section, an analytical formalism resulting to the acceleration of electrons by surface plasmon polaritons and their trajectories in both single and double metals configurations will be discussed.

5.5.1 Double Metal Configuration

Let an electron be injected into the middle of the vacuum region bounded by two metal surfaces (cf. Fig. 5.3), in the presence of large amplitude surface plasmon wave. The electron response is governed by the equation of motion [20]

$$\frac{d\vec{p}}{dt} = -e\left(\vec{E} + \vec{\mathrm{v}} \times \vec{\mathrm{B}}\right), \tag{5.59}$$

where $-e$, m are the electronic charge and mass and $\vec{B} = \left(\nabla \times \vec{E}\right)/i\omega$. Expressing $d/dt = \mathrm{v}_z\, d/dz$, the x and z components of Eq. (5.59) can be written as

$$\frac{dp_x}{dz} = \left[\frac{em\gamma}{p_z}\left(\frac{k_z}{\alpha_2}\right) + \frac{e}{\omega}\left(\alpha_2 - \frac{{k_z}^2}{\alpha_2}\right)\right](e^{\alpha_2 x} + e^{-\alpha_2 x})A_1^{'} \sin(\omega t - kz + \phi), \tag{5.60}$$

$$\frac{dp_z}{dz} = \begin{bmatrix} -\dfrac{em\gamma}{p_z}(e^{\alpha_2 x} - e^{-\alpha_2 x})\cos(\omega t - kz + \phi) \\ +\dfrac{e}{\omega}\dfrac{p_x}{p_z}\left(-\alpha_2 + \dfrac{{k_z}^2}{\alpha_2}\right)(e^{\alpha_2 x} + e^{-\alpha_2 x})\sin(\omega t - kz + \phi) \end{bmatrix} A_1^{'}, \tag{5.61}$$

where $A_1^{'} = A_1 e^{-(t-z/v_g)^2/2{\tau_L}^2}$, $\gamma = (1 + p^2/m^2c^2)^{1/2}$, $\mathrm{v_g}$ is the group velocity of the surface plasmon wave, ϕ is the initial phase of the wave and we have considered a Gaussian temporal profile of the SPPs amplitude with τ_L pulse width. These equations are supplemented with

$$\frac{dx}{dz} = \frac{p_x}{p_z}, \tag{5.62}$$

$$\frac{dt}{dz} = \frac{\gamma m}{p_z}. \tag{5.63}$$

We introduce dimensionless quantities: $A_1^{''} \to eA_1^{'}/m\omega_p c, X \to \omega_p x/c, Z \to \omega_p z/c$, $P_x \to p_x/(mc)$, $P_z \to p_z/(mc)$, $T \to \omega_p t$, $\Omega = \omega/\omega_P$, $q = k_z c/\omega_P$, $\mathrm{v}_g^{'} = \mathrm{v_g}/c$. In terms of these, Eqs. (5.60), (5.61), (5.62), and (5.63) can be written as follows

$$\frac{\partial P_x}{\partial Z} = \left[\frac{\gamma}{P_z}\left(\frac{q}{\alpha_2^{'}}\right) + \frac{1}{\Omega}\left(\alpha_2^{'} - \frac{q^2}{\alpha_2^{'}}\right)\right]\left(e^{\alpha_2^{'} X} + e^{-\alpha_2^{'} X}\right)A_1^{''} \sin(\Omega T - qZ + \phi), \tag{5.64}$$

$$\frac{\partial P_z}{\partial Z} = \begin{bmatrix} -\dfrac{\gamma}{P_z}\left(e^{\alpha_2^{'} X} - e^{-\alpha_2^{'} X}\right)\cos(\Omega T - qZ + \phi) \\ +\dfrac{1}{\Omega}\dfrac{P_x}{P_z}\left(-\alpha_2^{'} + \dfrac{q^2}{\alpha_2^{'}}\right)\left(e^{\alpha_2^{'} X} + e^{-\alpha_2^{'} X}\right)\sin(\Omega T - qZ + \phi) \end{bmatrix} A_1^{''}, \tag{5.65}$$

$$\frac{dX}{dZ} = \frac{P_X}{P_Z}, \tag{5.66}$$

$$\frac{dT}{dZ} = \frac{\gamma}{P_Z}. \tag{5.67}$$

We solve Eqs. (5.64), (5.65), (5.66), and (5.67) numerically for electron energy and electron trajectory. In Fig. 5.9a, b, we plotted kinetic energy (in keV) gained by the electrons versus normalized distance $z\,\omega_p/c$ for different values of laser frequency, for the parameters: $P_x(0) = 0.0$, $P_z(0) = 0.1$, $x(0) = 0.0$, $t(0) = 0.0$, $\tau_L\omega_P = 200$, $\varepsilon_L = 1, \phi = \pi/2, E_{SP} = 1.2 \times 10^{11}\, V/m$, $\omega_P = 1.3 \times 10^{16}\, rad/\sec$. Here we have taken width of vacuum gap $a\omega_P/c = 100$ i.e. $a = 231\,\mu m$ In Fig. 5.9a, we obtain electron acceleration of 12.7 keV for laser frequency $\omega/\omega_P = 0.06$ while in Fig. 5.9b, we obtained electron acceleration of 8.8 keV for $\omega/\omega_P = 0.087$. We note that with the increase in the frequency of the incident laser, electron acceleration decreases. This appears due to the increase in the phase velocity of the SPPs with increasing $|\varepsilon|$. The SPPs can accelerate electrons to the velocities of the order of phase velocity. The trajectory of the accelerated electron, launched in the centre of vacuum region turns out to be a straight line at $x = -a/2$, i.e., the electron moves in z-direction without deviation from its path. The trajectory of the accelerated electron in double metal surface is shown in Fig. 5.10a alongwith the trajectory of the accelerated electron over a single metal surface.

5.5.2 *Single Metal Configuration*

Consider an interface separating free space ($x > 0$) and a metal ($x < 0$). As discussed in Sect. 5.1, one can obtain the dispersion relation of the SPPs as

$$k_z^2 = \frac{\omega^2}{c^2}\frac{\varepsilon}{1+\varepsilon}, \tag{5.68}$$

where ε is the dielectric constant of the metal.

An electron beam is launched parallel to the surface with initial velocity $\vec{v}_0$. Its response to the surface plasmon polaritons is governed by the wave Eq. (5.59). The x and z components alongwith supplementary equations can be written as

$$\frac{\partial P_x}{\partial z} = A\left[-\frac{\gamma m e}{P_z}\left(\frac{k_z}{\alpha_1}\right)\sin(\omega t - k_z z + \phi) + \frac{e}{\omega}\left(\frac{k_z^2}{\alpha_1} - \alpha_1\right)\sin(\omega t - k_z z + \phi)\right] e^{-\alpha_1 x}, \tag{5.69}$$

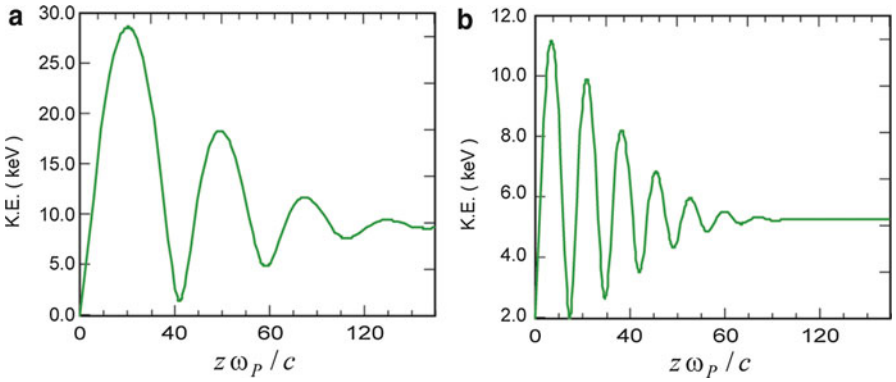

Fig. 5.9 Variation of kinetic energy of accelerated electrons, $(\gamma - 1)\, mc^2$ versus normalized distance $z\ \omega_P/c$ in double metal surface for two different laser frequencies (**a**) $\omega/\omega_P = 0.06$, and (**b**) $\omega/\omega_P = 0.087$. The other parameters are: $Px\ (0) = 0.0$, $Pz\ (0) = 0.009$, $x(0) = 0.1$, $t(0) = 0.0$, $\tau_L \omega_P = 200$, $\varepsilon_L = 1$, $\varphi = \pi/2$, $E_{SP} = 1.2 \times 10^{11}\, V/m$, $\omega_P = 1.3 \times 10^{16}\, rad/\sec$, $a\omega_P/c = 100$

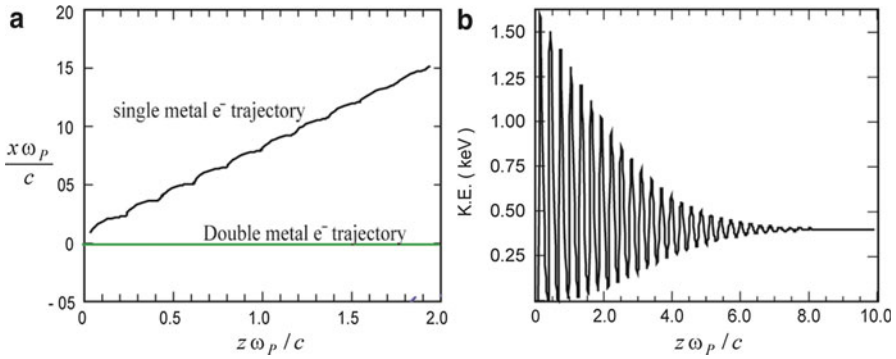

Fig. 5.10 (**a**) Trajectory of electron in single and double metal surface. (**b**) Variation of kinetic energy versus normalized distance $z\ \omega_P/c$ over the single metal surface. The parameters are: $Px\ (0) = 0.0$, $Pz\ (0) = 0.007$, $x(0) = 0.1$, $t(0) = 0.0$. $L_\tau = 27$ fs, $E = 10^6$ V/cm, $\varepsilon_L = 5$, $\omega = 375 THz$. $\varphi = \pi$

$$\frac{\partial P_z}{\partial z} = A\left[-\frac{\gamma m e}{P_z}\cos(\omega t - k_z z + \phi) - \frac{e}{\omega}\frac{p_x}{p_z}\left(\frac{k_z^2}{\alpha_1} - \alpha_1\right)\sin(\omega t - k_z z + \phi)\right] e^{-\alpha_1 x}, \tag{5.70}$$

$$\frac{dx}{dz} = \frac{p_x}{p_z}, \tag{5.71}$$

$$\frac{dt}{dz} = \frac{\gamma m}{p_z}. \tag{5.72}$$

where ϕ is the initial phase of the SPPs. Equations (5.69), (5.70), (5.71), and (5.72) in dimensionless form can be written as

$$\frac{\partial P_x}{\partial Z} = A'' \left[-\frac{\gamma}{P_z}\left(\frac{q}{\alpha_1'}\right) \sin(\Omega T - qZ + \phi) + \frac{1}{\Omega}\left(\frac{q^2}{\alpha_1'} - \alpha_1'\right) \sin(\Omega T - qZ + \phi) \right], \tag{5.73}$$

$$\frac{\partial P_z}{\partial Z} = A'' \left[-\frac{\gamma}{P_z} \cos(\Omega T - qZ + \phi) - \frac{1 P_x}{\Omega P_z}\left(\frac{q^2}{\alpha_1'} - \alpha_1'\right) \sin(\Omega T - qZ + \phi) \right], \tag{5.74}$$

$$\frac{dX}{dZ} = \frac{P_X}{P_Z}, \tag{5.75}$$

$$\frac{dT}{dZ} = \frac{\gamma}{P_Z}. \tag{5.76}$$

where, $A'' = A' e^{-\alpha_1' X} e^{-\left(T - Z/v_g'\right)^2 / 2\tau_L'^2}$, and X, Y and $\vec{P}$ are same as defined above.

We have solved these equations numerically for following parameters: $P_X(0) = 0.0$, $P_Z(0) = 0.007$, $X(0) = 1.0$, $T(0) = 0.0$, $\phi = \pi$. We express the surface plasmon wave amplitude as $|E_S| = \eta |E_L|$, where $|E_L|$ is the amplitude of the laser used to excite it in the attenuated total reflection (ATR) configuration and η is the enhancement factor. Presuming laser energy conversion to the SPPs as 50 %, enhancement factor comes out to be $\eta \cong 3.2$ corresponds to the laser intensity of 10^{13} W/cm^2. We choose $E_L = 2.9 \times 10^5$ V/cm. The results are displayed in Fig. 5.10a, b. The maximum kinetic energy gain by the electrons comes out to be ~ 0.39 KeV, which is close to the experimentally observed value of 0.4 KeV by Zawadzka et al. [21]. In Fig. 5.10a, we have plotted electron trajectory in x-z plane for the same parameters. One may note that the electron move away from the metal surface as it gains energy and hence not confined.

5.6 Surface Plasmon Excitations in Surface Enhanced Raman Spectroscopy

Surface enhanced Raman spectroscopy or surface enhanced Raman scattering (SERS) is an analytical technique that provides signals with enhanced intensity for Raman active molecule that have been adsorbed onto metal surface, patterns or nanostructures [22]. There are two main theories that explain the mechanism behind enhanced Raman scattering. One theory relies on the formation of charge complex and charge transfer [23] between chemisorbed species and the metal surface. The second theory believes that Raman enhancement occurs for the adsorbed material on a specific substrate (mainly metals or their nanocrystals) due to the enhancement of electric field provided by the substrate. There is generation of localized surface plasmons when a light beam is incident on substrate. In this case electric field enhancement is more at plasmon frequency [24].

Raman scattering is inelastic scattering of photon that often occurs when time harmonic field interacts with the molecular vibration. In this process, scattered radiation are also produced [24]. The frequency of this scattered radiation is little shifted from the incident radiation. Such a shift is equivalent to the vibrational frequency of the molecule. The origin of this vibrating frequency is oscillation between constituent atoms of the molecules. This oscillation and corresponding shift in frequency depends on molecular structure. The Raman scattering is weak effect and its scattering cross section order of magnitude is ~14–15 times smaller than the fluorescence cross section of an efficient dye [25]. Hence, field enhancement in many cases becomes very important. Such an enhancement factor is typically on the order of ~10^6. However, in some cases higher order enhancements were also achieved. In this chapter Raman signal enhancement from the enhanced electric fields at rough metal surface is discussed. Such an enhancement can be observed at places such as junction between metal crystals, grove, and cracks on the surfaces. The most common assumption is that Raman scattering enhancement is related to fourth power of electric field enhancement. Fig. 5.11 is shown to understand the phenomenon of SERS. Here a molecule is located at d_o, that is also in close proximity to metallic structure (local field enhancing device). There will be an interaction between incident field 'E_o' with the molecule, that result in a dipole moment associated with Raman scattering [25].

$$\mu(\omega_R) = \alpha(\omega_R + \omega)(E_o(d_o, \omega) + E_s(d, \omega)), \tag{5.77}$$

where, ω = frequency of the incident radiation, ω_R = A particular vibrationally shifted frequency ($\omega_R = \omega \pm \omega_{vib}$), α = polarizability (modulated at the vibrational frequency, ω_{vib}). Note that, there is an interaction of molecule with local field '$E_o + E_s$', here 'E_o' is the parent electric field, 'E_s' is the enhanced electric field due to interaction with nanostructures or pattern. E_s linearly depends on E_o, and can be represented as:

$$E_s = f_1(\omega).E_o,\ (f_1(\omega) = \text{field enhancement factor}) \tag{5.78}$$

The induced dipole (μ) radiated electric field can be written using Green's Function relation, after considering the presence of nano-structures [25]:

$$E(d_\infty, \omega_R) = \frac{\omega_R^2}{\varepsilon_o c^2} G(d_\infty, d_o)\mu(\omega_R). \tag{5.79}$$

Greens function can be split into a free space Green function 'G_o' (without any metal) and a scattered one 'G_s' (that originates from metallic nanostructure) [25]:

$$G(d_\infty, d_o) = G_o(d_\infty, d_o) + G_s(d_\infty, d_o), \tag{5.80}$$

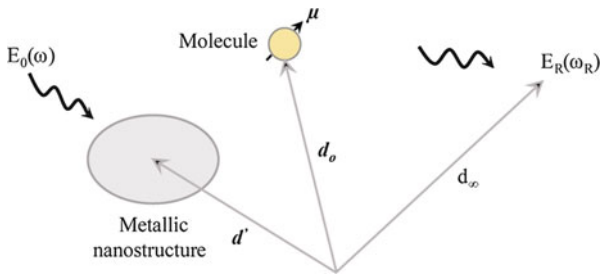

Fig. 5.11 An schematic representation of surface enhanced spectroscopy phenomenon. Here an interaction between a molecule (polarizability α) and the exciting electric field 'E_o' causes scattered Raman radiation with electric field E_R . The presence of metallic nanostructure in close proximity of molecule or compound of interest, enhances the exciting field as well as radiated field

$$G_s = f_2(\omega_R) G_o, \tag{5.81}$$

where $f_2(\omega_R)$ = second field enhancement factor. Now using above equations, intensity can be calculated, that is squared proportional to intensity [25]:

$$I(d_\infty, \omega_R) = \frac{\omega_R^4}{\varepsilon_o^2 c^4} |(1 + f_1(\omega_R))(1 + f_2(\omega_R)) G(d_\infty, d_o) \alpha(\omega_R, \omega)|^2 I_o(d_o, \omega). \tag{5.82}$$

Hence it can be said that Raman scattered intensity varies linearly with intensity I_o, with factor:

$$f_{overall} = |(1 + f_1(\omega_R))(1 + f_2(\omega_R))|^2. \tag{5.83}$$

Now, when there is no metal structures, the enhancement factors f_1 and f_2 are zero; whereas in the presence of metallic nanostructures these factors are very high compared to 1 and hence, overall scattering enhancement can be written as [25]:

$$f_{overall} = |f_1(\omega_R) f_2(\omega_R)|^2, \tag{5.84}$$

(Under the assumption that $|\omega_R \pm \omega|$ is smaller compared to the spectral response of the metal nanostructures.) Fig. 5.12 shows Raman spectra of rutile TiO_2 nanocrystalline film coated on glass as well as gold substrate. These examinations were carried using an R 3000 QE Raman spectrophotometer at backscattering mode. The excitation wavelength was ~785 nm and laser power was ~100 mW. The peaks were observed at ~448 cm^{-1} and 611 cm^{-1}. It can be observed that peak intensity for TiO_2 coated on Au back substrate was several times higher compared to that coated on glass substrate.

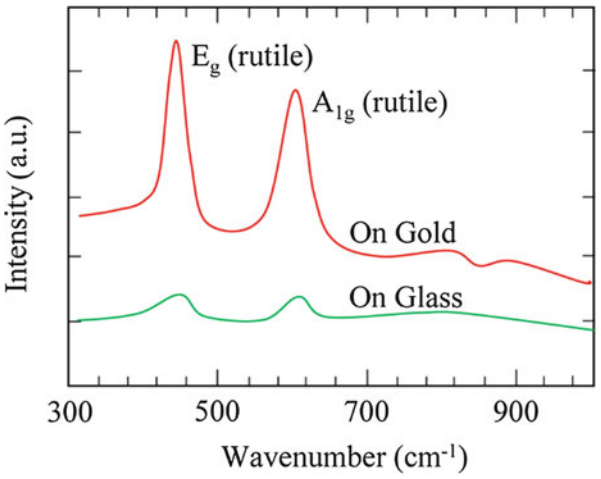

Fig. 5.12 Raman spectra of rutile TiO_2 nanocrystalline film coated on glass and gold substrate. The height of spectral features is several times higher when Au is used as a back contact. This is caused by the surface enhanced Raman scattering phenomenon

5.7 Surface Plasmon Plasmon Applications in Sensing and Solar Cell Technology

Surface plasmons and their associated resonance condition have been widely utilized in various sensing devices [26]. These groups of surface plasmons based refractometric sensing devices are one of the main sensing technique, used for biological species and chemical detections. In most of the cases these are SPR based refractometer that measure any variation in refractive index at metal film surface. Any change in refractive index of dielectric medium causes a change in surface plasmon propagation constant [26]. The change in coupling condition (coupling intensity, phase, wavelength, coupling angle) can be utilized for probing. For example, in case of angular modulation based SPR sensors, a monochromatic light wave is generally utilized for surface plasmons excitation [26]. Coupling strength between surface plasmon and incident light wave can be observed at multiple angles of incidence by using convergent light beam. For evaluating sensor output, the angle of incidence giving strongest coupling, is measured. In contrast, SPR sensor working on wavelength modulation, surface plasmons are generally excited using collimated light wave with multiple wavelengths. These SPR based sensors have been extensively used in detection of pathogens, toxins, hormones, proteins, vitamins, and diagnostic antibodies [26].

Surface plasmons have been widely utilized for effective light management in order to achieve high efficiency of photovoltaic devices with thin absorber layer [27]. Use of thin film is advantageous because it reduces material cost. Additionally, for such thin film solar cells, performance can be enhanced and in certain cases, efficiency can be improved if adequate light can be scattered inside the absorber layer film using metallic nanoparticles [27]. In many cases, surface texturing has been used to improve a short circuit current. However, surface recombination and difficulties in fabrication of good quality semiconducting layers

in such cases have been a challenge. Enhanced light trapping in absorber layer can be achieved by tuning localized surface plasmons in arrays of Au or Ag nanocrystals [28]. Both thin film and wafer based Si solar cells have shown increased performance due to the presence of Ag nanoparticles. The main mechanisms that explain photocurrent enhancement by metallic nanoparticles are light scattering and near field concentration of light [27, 28]. The size of particle and electrical/optical properties of semiconductor absorber layer are factors that decide the contribution from each mechanism. The power conversion efficiency of ~15.3 % using metallic nanoparticles but only using ~18 μm thick Si layer, was reported [29]. It saves ~97 % of the absorber materials. Apart from Si, nanoparticles have also been utilized in organic bulk hetrojunction solar cells, hybrid solar cells, and perovskite materials, for efficiency improvement [30].

Acknowledgements Authors would like to greatly acknowledge Prof. V.K. Tripathi for his valuable guidance and inspiring discussions during the course of work reported in this chapter.

References

1. (a) Zayats AV, Smolyaninov II, Maradudin AA (2005) Nano-optics of surface plasmon polaritons. Phys Rep 408(3):131–314; (b) Raether H (1988) Surface plasmons on smooth surfaces. Springer, Berlin Heidelberg; (c) Agranovich VM, Mills DL (1982) Surface Polaritons. Elsevier, North-Holland, Amsterdam.
2. Wood R (1902) XLII. On a remarkable case of uneven distribution of light in a diffraction grating spectrum. Lond Edinb Dublin Philos Mag J Sci 4(21):396–402
3. Wood RW (1902) On a remarkable case of uneven distribution of light in a diffraction grating spectrum. Phil Mag 4:396–402
4. Fano U (1941) The theory of anomalous diffraction gratings and of quasi-stationary waves on metallic surfaces (Sommerfeld's waves). JOSA 31(3):213–222
5. Otto A (1968) Excitation of nonradiative surface plasma waves in silver by the method of frustrated total reflection. Z Phys 216(4):398–410
6. Kretschmann E, Raether H (1968) Radiative decay of non-radiative surface plasmons excited by light. Z Naturforsch A 23(12):2135–2136
7. Okamoto K, Niki I, Shvartser A, Narukawa Y, Mukai T, Scherer A (2004) Surface-plasmon-enhanced light emitters based on InGaN quantum wells. Nat Mater 3(9):601–605
8. (a) Barnes WL, Dereux A, Ebbesen TW (2003) Surface plasmon subwavelength optics. Nature 424(6950):824–830; (b) Genet C, Ebbesen T (2007) Light in tiny holes. Nature 445 (7123):39–46; (c) Klimov V, Ducloy M, Letokhov V (2002) A model of an apertureless scanning microscope with a prolate nanospheroid as a tip and an excited molecule as an object. Chem Phys Lett 358(3):192–198; (d) Krupin O, Asiri H, Wang C, Tait RN, Berini P (2013) Biosensing using straight long-range surface plasmon waveguides. Opt Express 21(1): 698–709
9. Saito H, Namura K, Suzuki M, Kurata H (2014) Dispersion relations for coupled surface plasmon-polariton modes excited in multilayer structures. Microscopy 63(1):85–93
10. Sheng P, Stepleman RS, Sanda PN (1982) Exact eigenfunctions for square-wave gratings: application to diffraction and surface-plasmon calculations. Phys Rev B 26(6):2907–2916
11. Stockman MI, Faleev SV, Bergman DJ (2001) Localization versus delocalization of surface plasmons in nanosystems: can one state have both characteristics? Phys Rev Lett 87(16):167401

12. Davis TJ (2009) Surface plasmon modes in multi-layer thin-films. Opt Commun 282(1):135–140
13. Stoian R, Rosenfeld A, Ashkenasi D, Hertel I, Bulgakova N, Campbell E (2002) Surface charging and impulsive ion ejection during ultrashort pulsed laser ablation. Phys Rev Lett 88 (9):097603
14. (a) Kumar G, Tripathi V (2007) Anomalous absorption of surface plasma wave by particles adsorbed on metal surface. Appl Phys Lett 91(16):161503; (b) Mishra Y, Adelung R, Kumar G, Elbahri M, Mohapatra S, Singhal R, Tripathi A, Avasthi D (2013) Formation of self-organized silver nanocup-type structures and their plasmonic absorption. Plasmonics 8 (2):811–815
15. Vorobyev A, Guo C (2005) Enhanced absorptance of gold following multipulse femtosecond laser ablation. Phys Rev Ser B 72(19):195422
16. (a) Wolfbeis OS (2006) Fiber-optic chemical sensors and biosensors. Anal Chem 78(12):3859–3874; (b) Chau L-K, Lin Y-F, Cheng S-F, Lin T-J (2006) Fiber-optic chemical and biochemical probes based on localized surface plasmon resonance. Sensors Actuators B Chem 113(1):100–105
17. Homola J, Yee SS, Gauglitz G (1999) Surface plasmon resonance sensors: review. Sens Actuators B 54(1):3–15
18. (a) Lucotti A, Zerbi G (2007) Fiber-optic SERS sensor with optimized geometry. Sensors Actuators B Chem 121(2):356–364; (b) Liu C, Kumar G, Tripathi V (2006) Laser mode conversion into a surface plasma wave in a metal coated optical fiber. J Appl Phys 100 (1):013304
19. Liu CS, Tripathi VK (1998) Diffraction-limited laser excitation of a surface plasma wave and its scattering on a rippled metallic surface. Quantum Electron IEEE J 34(8):1503–1507
20. Liu C, Kumar G, Singh D, Tripathi V (2007) Electron acceleration by surface plasma waves in double metal surface structure. J Appl Phys 102(11):113301
21. Zawadzka J, Jaroszynski DA, Carey JJ, Wynne K (2001) Evanescent-wave acceleration of ultrashort electron pulses. Appl Phys Lett 79(14):2130–2132
22. (a) Schlücker S (2014) Surface-enhanced Raman spectroscopy: concepts and chemical applications. Angew Chem Int Ed 53(19):4756–4795; (b) Kumar G, Singh D, Tripathi V (2006) Surface enhanced Raman scattering of a surface plasma wave. J Phys D Appl Phys 39(20):4436
23. Lombardi JR, Birke RL, Lu T, Xu J (1986) Charge-transfer theory of surface enhanced Raman spectroscopy: Herzberg–Teller contributions. J Chem Phys 84(8):4174–4180
24. Moskovits M (2005) Surface-enhanced Raman spectroscopy: a brief retrospective. J Raman Spectrosc 36(6–7):485–496
25. Novotny L, Hecht B (2012) Principles of nano-optics. Cambridge University Press, Cambridge
26. Homola J (2008) Surface plasmon resonance sensors for detection of chemical and biological species. Chem Rev 108(2):462–493
27. Catchpole KR, Polman A (2008) Design principles for particle plasmon enhanced solar cells. Appl Phys Lett 93(19):191113
28. Beck FJ, Polman A, Catchpole KR (2009) Tunable light trapping for solar cells using localized surface plasmons. J Appl Phys 105(11):114310
29. Zhang Y, Stokes N, Jia B, Fan S, Gu M (2014) Towards ultra-thin plasmonic silicon wafer solar cells with minimized efficiency loss. Sci Rep 4:4939
30. (a) Lee JH, Park JH, Kim JS, Lee DY, Cho K (2009) High efficiency polymer solar cells with wet deposited plasmonic gold nanodots. Org Electron 10(3):416–420; (b) Zhou F, Zhu J, Lai Z, Liu Y, Zhao X (2014) Surface plasmon resonances behavior in visible light of non-metal perovskite oxides AgNbO3. Appl Phys Lett 105(23): 231121